Available online at www.sciencedirect.com
SCIENCE DIRECT
Journal of Molecular Catalysis A: Chemical 237 (2005) 172–181
JOURNAL OF MOLECULAR CATALYSIS A: CHEMICAL
www.elsevier.com/locate/molcata

Effect of magnesia on alumina-supported cobalt Fischer–Tropsch synthesis catalysts

Yuhua Zhang, Haifeng Xiong, Kongyong Liew, Jinlin Li *

Hubei Key Laboratory for Catalysis and Material Science, College of Chemistry and Material Science, South-Central University for Nationalities, Wuhan 430074, China

Received 23 January 2005; received in revised form 11 April 2005; accepted 20 April 2005
Available online 13 June 2005

Abstract

A series of magnesia-modified alumina-supported cobalt catalysts were prepared with a two-step impregnation method using the incipient wetness technique. N_2 physisorption, X-ray diffraction (XRD), laser Raman spectroscopy (LRS), X-ray photoelectron spectroscopy (XPS), H_2 temperature-programmed reduction (H_2-TPR), H_2 temperature-programmed desorption (H_2-TPD) and oxygen titration were used for the characterization of the catalysts. A cobalt surface phase, which has strong interaction with the support, was detected by XPS, and its content decreased with introduction of the magnesia into the catalysts, indicating that Mg modification can inhibit the interaction between the cobalt oxide and the support. However, large amounts of magnesia caused a decrease in the catalysts reducibility due to the formation of MgO–CoO solid solution. Small amounts of magnesia were found to improve the activity of cobalt catalysts for Fischer–Tropsch synthesis but larger amounts of magnesia decreased the activity, and the methane and CO_2 selectivity increased for all the magnesia-modified catalysts; furthermore, the olefin to paraffin ratio increased with an increase in magnesia content. These observed effects of magnesia on the catalytic performance of cobalt catalysts could deduce from poor reducibility of higher magnesia content catalysts and/or magnesia content-dependent catalyst surface reconstruction suppression.

Keywords: Fischer–Tropsch synthesis; Cobalt; Alumina; Magnesia; Modification

1. Introduction

Fischer–Tropsch synthesis (FTS) attracts great attention as an option for clean transportation fuels and chemicals' production via natural gas or cheap coal [1,2]. Fe, Co, Ni and Ru are typical FTS catalysts [1–3]. Recent interest in FTS catalysts for diesel fuel production from natural gas has concentrated on supported cobalt catalysts because of their high activity and selectivity for heavy waxy product at low temperature FTS, lower water–gas shift reaction activity with hydrogen-rich syngas as produced from natural gas than iron catalysts and lower price than noble metals, as ruthenium [1,3].

The effect of support on cobalt FTS catalysts, such as Al_2O_3, TiO_2, SiO_2, C and MgO, etc., has been investigated [4–7]. Alumina is often used as a support for cobalt FTS catalysts due to its favorable mechanical properties, but an alumina-supported catalyst has a limited reducibility due to a strong interaction between the support and the cobalt oxides [8–12]. The cobalt species, which strongly interact with the support, are generally inactive in CO hydrogenation due to their low reducibility. This can be improved to a certain extent by adding metal or metal oxide promoters, such as Pt [13], Re [14], ZrO_2 [15], etc.

The interaction between the support and the cobalt oxides depends largely on the chemical and physical properties of the support as well as the cobalt loading. This may result in the formation of stoichiometric or non-stoichiometric cobalt aluminate spinel when alumina was used [12,16]. Modification of the support surface may suppress the interaction. A number of investigations have been focused on magnesia as a modifier for the cobalt-based catalysts [17–22]. Studies on the possibility of inhibiting the interaction between

* Corresponding author. Tel.: +86 27 67843016; fax: +86 27 67842752.
E-mail address: lij@scuec.edu.cn (J. Li).

1381-1169/$ – see front matter © 2005 Elsevier B.V. All rights reserved.
doi:10.1016/j.molcata.2005.04.057

the cobalt oxide and the support by adding magnesia to an alumina support has shown that the magnesia modification increased not only the reducibility of cobalt oxide but also the catalytic activity in CO hydrogenation [17]. The investigation of Co–Mg–Al layered double hydroxides showed that the magnesia could decrease the amount of a non-stoichiometric Co–Al spinel phase [23]. Lahtinen and Somorjai [24] studied carbon monoxide hydrogenation on polycrystalline cobalt foils; they concluded that Mg reduced the methane selectivity and increased the C_4 and C_5 hydrocarbons selectivities. On the other hand, the presence of magnesia decreased the reducibility of SiO_2-supported cobalt catalysts [18] and cobalt-kieselguhr catalysts [19] but increased the dispersion of cobalt on the SiO_2 [18,22]. In addition, the order of impregnation of magnesia and cobalt can also affect the activity and selectivity of the magnesia promoted catalysts [18]. However, the intrinsic effect of modification of the support by magnesia on the metal–support interaction, the reducibility, the activity and selectivity of the cobalt catalysts for FTS are still unclear.

It has been discovered that the presence of water vapor during FTS reaction can enhance the deactivation of cobalt-based catalysts due to surface oxidation or compound formation between the metal and the support [10,13,25]. A series of works in our group was concerned with the effect of modification of the support by metal oxide, such as zirconia [26] and magnesia on the deactivation of cobalt-based catalysts for FTS. In the present work, a series of magnesia-modified Co/Al_2O_3 catalysts were prepared and characterized by N_2 physisorption, X-ray diffraction (XRD), laser Raman spectroscopy (LRS), X-ray photoelectron spectroscopy (XPS), H_2 temperature-programmed reduction (H_2-TPR), H_2 temperature-programmed desorption (H_2-TPD) and oxygen titration, and their catalytic performances were tested in a fixed bed reactor. The aim is to investigate the effect of magnesia as a modifier for alumina on the metal–support interaction, activity and selectivity of cobalt catalysts, and further work is needed to identify the intrinsic effect of the modification on the deactivation of the catalysts due to the water vapor.

2. Experimental

2.1. Materials

2.1.1. Co/Al_2O_3

The alumina-supported cobalt catalyst (Co/Al_2O_3) was prepared with the incipient wetness impregnation using a cobalt nitrate aqueous solution. The support (γ-Al_2O_3, 415#, Shandong Aluminum Co., China; BET surface area: 221.03 $m^2\,g^{-1}$; pore volume: 0.53 $cm^3\,g^{-1}$; particle size: 0.4–0.6 mm) was first calcined at 873 K for 5 h before impregnation. A two-step impregnation was used with drying at 353 K in a rotary evaporator and then drying at 393 K for 12 h in an oven following each impregnation. After the final impregnation and drying, the catalyst was calcined in a furnace at 623 K for 5 h.

2.1.2. $Co/MgO/Al_2O_3$

The magnesia-modified alumina-supported cobalt catalysts ($Co/MgO/Al_2O_3$) were prepared with the sequential incipient wetness impregnation method. Firstly, magnesia-modified supports were prepared by impregnating magnesium nitrate aqueous solution onto the same support (Al_2O_3) as mentioned above (in the case of 9 and 12 wt% of MgO content, a two-step impregnation was used due to the limited solubility of the magnesium nitrate). After each impregnation, the magnesia-modified alumina supports were dried at 393 K overnight in air and calcined at 823 K for 5 h in air. Then, the $Co/MgO/Al_2O_3$ catalysts were prepared using the same procedure as for the Co/Al_2O_3 catalyst.

The catalysts used in this paper are denoted as 15CoA or 15Co*X*MA; 15 refers to 15 wt% of cobalt loading in the catalysts, A refers to the Al_2O_3 support, MA refers to the magnesia-modified alumina supports, and *X* refers to the magnesium content in MA. The compositions of the catalyst are shown in Table 1.

2.1.3. Reference samples

$CoAl_2O_4$ (spinel) was prepared by calcining 15CoA at 1273 K for 10 h, and Co_3O_4 was obtained by calcining cobalt nitrate at 1073 K for 8 h.

2.2. Catalyst characterization

2.2.1. N_2 physisorption

The BET surface area, pore volume, average pore diameter and pore size distribution of the catalysts were determined by N_2 physisorption using a Micromeritics ASAP 2405 automatic system. Each sample was degassed at 10^{-6} Torr at 473 K for 4 h prior to N_2 physisorption.

2.2.2. X-ray diffraction

The XRD measurement was performed on a Philips X'pert Pro Powder Diffractometer with Cu Kα radiation. The spectra were scanned with a rate of 0.002° min^{-1} from 10° to 90° (2θ). The identification of the phases was made with the

Table 1
Catalyst compositions

Samples name	MgO (wt%)[a]	Co (wt%)[b]	Bulk molar ratio (Mg/Al)	Surface molar ratio (Mg/Al)[c]
15CoA	–	15.00	–	–
15Co03MA	0.40	15.00	0.01	–
15Co08MA	1.06	15.03	0.02	0.13
15Co2MA	2.69	15.02	0.04	0.15
15Co5MA	6.68	15.00	0.11	0.23
15Co9MA	12.04	15.00	0.22	0.45
15Co12MA	15.87	15.00	0.31	–

[a] Magnesia content (wt%) in the prepared catalysts.
[b] Cobalt content (wt%) in the prepared catalysts.
[c] Obtained by XPS measurement.

help of the Joint Committee on Powder Diffraction Standards files (JCPDS). The average Co_3O_4 crystallite size of the catalysts was calculated using the Sherrer equation [27]. The diameter of a given Co_3O_4 particle could be used to calculate the diameter of metallic Co crystallite by the formula below [28]:

$$d_{Co} = 0.75 d_{Co_3O_4}$$

2.2.3. Laser Raman spectroscopy

The LRS spectra of the samples were collected using a Confocal Renishaw Raman Microprobe RM-1000 by projecting a continuous wave laser of argon ion (Ar^+) (514.5 nm) through the samples exposed to air at room temperature. A count time of 30 s at focus with a 50 times objective lens and a scanning range between 80 and 2200 cm^{-1} with a resolution of 2 cm^{-1} was applied.

2.2.4. X-ray photoelectron spectroscopy

The XPS spectra were recorded using a Physical Electronics PHI-5800 spectrometer with a monochromatized Al Kα source (1486.6 eV). The C 1s line (284.6 eV) was taken as a reference to correct for electrostatic charging. In order to determine the intensity of the different cobalt species on the samples, the recorded Co 2p regions were fitted, and 80% Gaussian and 20% Lorentzian peaks were used in the peak deconvolution.

2.2.5. H_2 temperature-programmed reduction, H_2 temperature-programmed desorption and oxygen titration

H_2-TPR was carried out using a Zeton Altamira AMI-200 system with a 10% H_2/Ar mixture referenced to Ar. It was conducted using 150 mg of catalyst and a temperature ramp from 323 to 1073 K at 10 K per minute. A thermal conductivity detector (TCD) was used to determine the amount of hydrogen consumed.

The amount of H_2 chemisorption was measured with H_2-TPD using a Zeton Altamira AMI-200 system. The catalyst samples were reduced using hydrogen at 723 K for 12 h and cooled under flowing H_2 to 373 K. Then, the samples were held at 373 K under flowing Ar to remove physisorbed and/or weakly bound species prior to increasing the temperature slowly to the reduction temperature. At that temperature, the catalysts were held under flowing Ar to desorb the remaining chemisorbed H_2. The TPD spectra were integrated and the number of moles of desorbed H_2 was determined by comparing to the areas of calibration pulses of H_2 in Ar.

The reduction level of the catalysts was determined by oxygen titration. After the H_2-TPD, the samples were reoxidized at the reduction temperature by pulses of pure O_2 in He carrier referenced to He. After reoxidation of the reduced catalysts, the number of moles of O_2 consumed was determined using a TCD. The percentage reduction (Red.%) was calculated by assuming stoichiometric conversion of metallic Co to Co_3O_4. The percentage dispersion (*D*%) was calculated according to the equation [29]:

$$D\% = \frac{1.179X}{W\text{Red.}\%}.dy$$

where *X* is the amount of chemisorbed H_2 in micromoles per gram of catalysts, *W* is the weight percent of cobalt. It should be noted here that, with the introduction of reduction degree, the unreduced cobalt oxide was not included in the calculation of *D*%. The importance of the correction by introducing the percentage reduction into the calculation of dispersion has been stressed by Jacobs et al. [5]. The average crystallite diameters of Co were calculated from *D*% assuming spherical metal crystallite of uniform diameter *d* with a site density of 14.6 atoms/nm^2 [29].

$$d_{Co} = \frac{96}{D\%}$$

2.3. Fischer–Tropsch synthesis

FTS was carried out in a down-flow fixed-bed stainless-steel reactor (i.d. 2.5 cm). The 6 g of catalysts, which were diluted by 36 g of quartz (200–460 mesh) and 80 g of glass bead (diameter of 4–6 mm) to minimize the temperature gradients, was charged into the reactor. The temperature was controlled using a three-zone furnace. A thermocouple was placed at the middle of the catalyst bed to assure a precise temperature control during pretreatment and the reaction process. The mass flow controllers (Brooks 5850E) were used to control the flow rate of H_2 and syngas. Prior to the FTS, the catalysts were reduced in flowing H_2 at 723 K and the atmospheric pressure for 12 h; the space velocity of H_2 was 6 N L g^{-1} h^{-1} (298 K, 0.1 MPa). After reduction, the catalysts were cooled to 453 K in flowing H_2. Then, the syngas (H_2/CO = 2) was introduced and the pressure was increased to 10 bar. The reaction temperature was then slowly increased to 503 K (453–483 K for 3 h and 483–503 K for 4 h), and the space velocity of syngas was 2 S L g^{-1} h^{-1} (273 K, 0.1 MPa). Preliminary experiments in our group show that steady state has been reached after an initial reaction of 24 h under the reaction condition, and then subsequent procedure below was conducted after the initial reaction. The duration of sampling was more than 50 h to achieve a good mass balance at the steady state.

The wax and water mixture were collected from the warm trap (403 K), and the oil plus water were collected from the cold trap (273 K). The wax was dissolved in dimethylbenzene and was analyzed using an Agilent 4890 GC with a FID detector, and the oil was analyzed using an Agilent 6890N GC with a FID detector. Tail gas from the cold trap was analyzed using an on-line Agilent Micro GC3000 with a TCD detector.

The carbon monoxide conversion (X_{CO}%) and the hydrocarbon selectivities were calculated based on the gas product analysis and the gas flow measuring results at steady state.

The olefin to paraffin ratio was calculated from the respective chromatographic peak areas.

3. Results and discussion

3.1. Texture of the catalyst

The BET surface area, total pore volume and average pore diameter of the catalysts are shown in Table 2. The surface area and the total pore volume decrease with increasing magnesia content, while the average pore diameter increases slightly indicating that the small pores of the Al_2O_3 support are blocked by magnesia.

3.2. X-ray diffraction

XRD profiles of $CoAl_2O_4$, Co_3O_4 and the catalysts are shown in Figs. 1 and 2. For all the catalysts, the cobalt species is present mainly in the form of spinel Co_3O_4, but no MgO phase was detected for the magnesia-modified catalysts (see Fig. 1), indicating that the MgO is highly dispersed on the alumina support [30]. The average crystallite size of Co_3O_4 increases slightly with increasing magnesia content, indicating that magnesia has minimal effect on the dispersion of cobalt (see Table 5). It can also be seen that the different catalysts display almost the same peak intensities. It is difficult to determine the $CoAl_2O_4$ phases for those catalysts based on the XRD characteristic alone because both Co_3O_4 and $CoAl_2O_4$ have cubic spinel structure with almost identical diffraction peak positions (see Fig. 2), and the Co–support compound formation could not be detected by X-ray diffraction [31]. Nevertheless, this can be resolved by LRS and XPS technique.

3.3. Laser Raman spectroscopy

The Raman spectra of reference samples and the catalysts are shown in Fig. 3. Alumina and magnesia themselves are not Raman active [32]; thus, no Raman spectroscopy signals can be seen. As can be seen, the Raman spectra of the unmodified and low-magnesia content catalysts show the same characteristic signals of Co_3O_4, suggesting that the surface of catalysts is covered with relatively large Co_3O_4 particles. This result is in agreement with the XRD measurements. With increasing magnesia content, all of the Raman bands of Co_3O_4 broaden, weaken noticeably and shift to lower frequencies. This suggests that the Co_3O_4 phase in the surface of the high-magnesia content catalysts have changed somewhat due to the addition of magnesia and the different cobalt oxide–support interactions, although the XRD data indicate that Co_3O_4 is still the main phase. This can be explained by the fact that LRS can only detect species on the sample surface with a thickness of about 2 nm, but XRD can detect the bulk phase in the cata-

Table 2
N_2 physisorption results

Samples name	BET surface area ($m^2\ g^{-1}$)	Pore volume ($cm^3\ g^{-1}$)	Average pore diameter (nm)
15CoA	143.87	0.377	10.48
15Co08MA	136.89	0.369	10.79
15Co5MA	119.02	0.324	10.89
15Co9MA	106.95	0.262	9.82

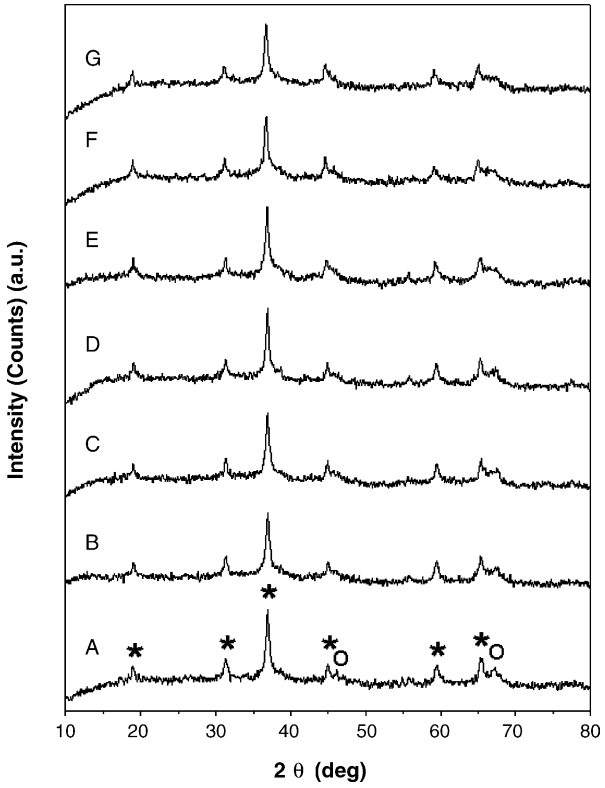

Fig. 1. XRD profiles of the prepared catalysts: (A) 15CoA; (B) 15Co03MA; (C) 15Co08MA; (D) 15Co2MA; (E) 15Co5MA; (F) 15Co9MA; (G) 15Co12MA; (✱) Co_3O_4; (◯) γ-Al_2O_3.

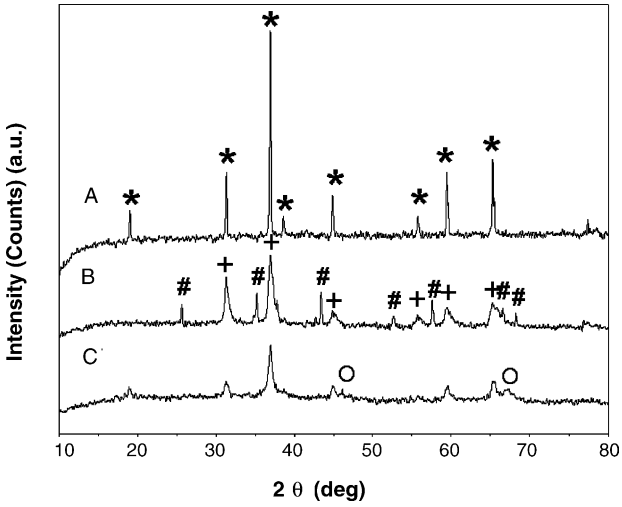

Fig. 2. XRD profiles of: (A) Co_3O_4; (B) $CoAl_2O_4$; (C) 15CoA; (✱) Co_3O_4; (#) α-Al_2O_3; (◯) γ-Al_2O_3; (+) $CoAl_2O_4$.

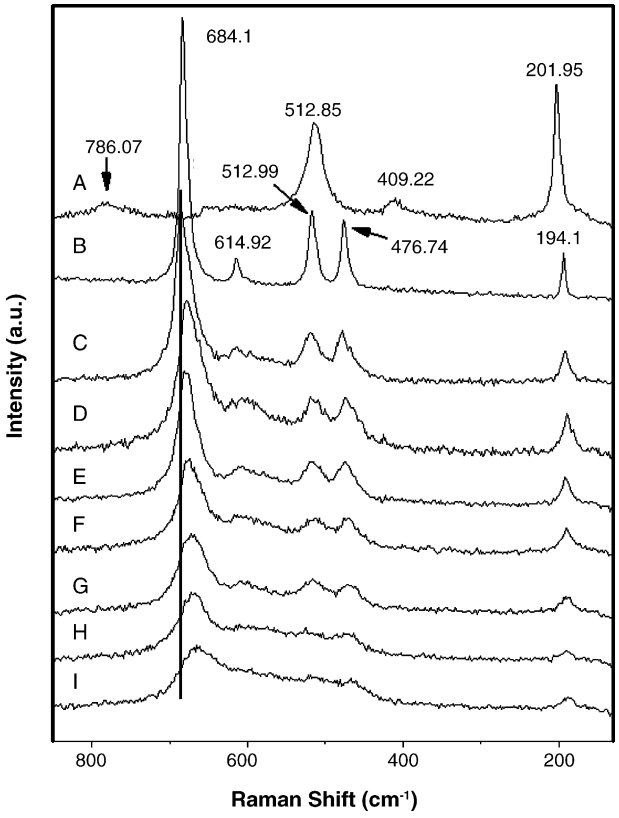

Fig. 3. Raman spectra of the reference samples and the prepared catalysts: (A) $CoAl_2O_4$; (B) Co_3O_4; (C) 15CoA; (D) 15Co03MA; (E) 15Co08MA; (F) 15Co2MA; (G) 15Co5MA; (H) 15Co9MA; (I) 15Co12MA.

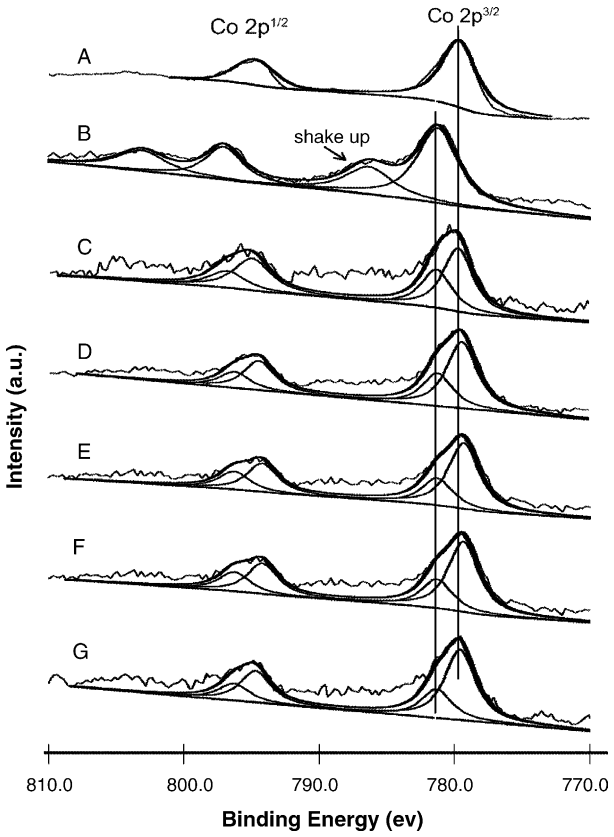

Fig. 4. The Co 2p XPS spectra of the reference samples and the prepared catalysts: (A) Co_3O_4; (B) $CoAl_2O_4$; (C) 15CoA; (D) 15Co08MA; (E) 15Co2MA; (F) 15Co5MA; (G) 15Co9MA.

lyst. It might be pointed out that the formation of CoO–MgO mixed phase on the magnesia-modified catalysts surface cannot be excluded [32,33].

It can also be seen that no characteristic Raman bands corresponding to $CoAl_2O_4$, which is related to a sharp, intense signal at 201.95 cm^{-1}, a broad bands at 512.85 cm^{-1} and two weak bands at 409.22 and 786.07 cm^{-1}, exist in the spectra of any of the prepared catalysts. This indicates that none or very little $CoAl_2O_4$ was formed during the pretreatment. However, it does not imply the absence of the strong interaction between the cobalt and the support.

3.4. Surface spectroscopic analysis

X-photoelectron spectroscopy was used in an attempt to obtain more insight into the surface composition of $Co/MgO/Al_2O_3$ catalysts. The XPS spectra of the Co 2p regions for the catalysts are shown in Fig. 4. The $CoAl_2O_4$ and Co_3O_4 spectra are included for reference. The peaks of Co 2p have been deconvolved for all the samples and the XPS analytical results on Co $2p^{3/2}$ binding energies are shown in Table 3, followed by the literature data of various Co-containing compounds in Table 4. It can be seen from Fig. 4 that the main peaks (Co $2p^{3/2}$,Co $2p^{1/2}$) of pure $CoAl_2O_4$ exhibit a shoulder at their high-energy side while that of Co_3O_4 peaks are remarkably weak. It is due to the shake-

Table 3
Co $2p_{3/2}$ binding energy (BE) of different compounds and the relative intensity ratios of cobalt surface phase to Co_3O_4 ($I_{CSP}/I_{Co_3O_4}$) for the catalysts

Samples name	Co $2p^{3/2}$ BE (eV)			$I_{CSP}/I_{Co_3O_4}$
	Co_3O_4 BE	$CoAl_2O_4$ BE	CSP[a] BE	
Co_3O_4	779.66	–	–	–
$CoAl_2O_4$	–	781.25	–	–
15CoA	779.69	–	781.30	0.62
15Co08MA	779.60	–	781.34	0.41
15Co2MA	779.34	–	781.30	0.41
15Co5MA	779.75	–	781.40	0.50
15Co9MA	779.40	–	781.20	0.49

[a] Cobalt surface phase.

Table 4
The XPS data and characteristics of the cobalt-containing reference materials [37]

Materials	Co $2p^{3/2}$ BE (eV)	Reliability (eV)	Shake-up satellite
Co_3O_4	780.0	±0.7	Weak
$CoAl_2O_4$	781.9	±0.5	Strong
CoO	780.1	±0.9	Strong
$Co(OH)_2$	780.9	±0.2	Strong
$Co(NO_3)_2$	781.9	–	Strong

up process of Co^{2+} in the high-spin state, but the low-spin Co^{3+} ion does not show a shake-up process [19,34]. Comparison of peaks shape and binding energy reveals that the magnesia-modified cobalt catalysts closely resemble Co_3O_4 whereas the peaks shape and binding energy of 15CoA catalyst are intermediate between that of $CoAl_2O_4$ and Co_3O_4. These results indicate that the addition of magnesia modifies the surface characteristics of alumina-supported cobalt catalyst.

The Co $2p^{3/2}$ peaks at about 779.6 eV indicate that most of the surface cobalt is Co_3O_4 for all the catalysts. Although the binding energy of the peaks at about 781.3 eV is similar to that of Co $2p^{3/2}$ peak of $CoAl_2O_4$, these peaks may be related to a cobalt surface phase (CSP) rather than $CoAl_2O_4$ [35–37] because of the weaker, or the absence of shake-up satellite.

The CSP was believed to be highly dispersed on the support after calcination and presumably present in monolayer thickness [36]. The Raman spectroscopic results also suggested that the surface cobalt–support compound was not identical to $CoAl_2O_4$ (spinel) but was probably a surface compound deficient in Co [31]. It can be concluded that the strong interaction between the CSP and the support is very favorable, and the formation of cobalt–support compound is facile.

Since all the XPS spectra were synthesized under the same fitting method, the relative intensity ratio of the different peaks obtained can represent the relative content of the different species. It can be seen from Table 3 that the relative intensity ratio of CSP to Co_3O_4 decreases with introduction of magnesia into the catalysts, indicating that the addition of magnesia inhibits the formation of cobalt surface phase; thus, the strong interaction between the cobalt species and the support is presumably suppressed.

3.5. Catalyst reducibility

The H_2-TPR profiles of the prepared catalysts are shown in Fig. 5. All the TPR profiles show two major regions: a lower temperature region located between 473 and 723 K and a higher temperature region located between 723 and 1073 K. For the unmodified catalyst (15CoA), the TPR peak at around 623 K is related to the two-step reduction $Co_3O_4 \rightarrow CoO \rightarrow Co^0$, which usually exhibits only one TPR peak [5], while the broad peak between 673 and1073 K is related to the reduction of cobalt oxide species (Co^{2+} and Co^{3+}), which strongly interact with the support [5], or the amorphous surface cobalt–support compounds [16]. The peak at around 553 K for 15CoA can be attributed to the reductive decomposition of some cobalt nitrate remaining in the catalyst after calcination. For all the magnesia-modified cobalt catalysts, the TPR peaks at 473–573 K are more intense than that of 15CoA, and the peaks at around 623 K are much narrow and more intense for 15Co9Mg and 15Co12Mg. It is suggested that the enhanced thermal stability of NO_3^- in magnesia-modified catalysts is due to the higher local charge

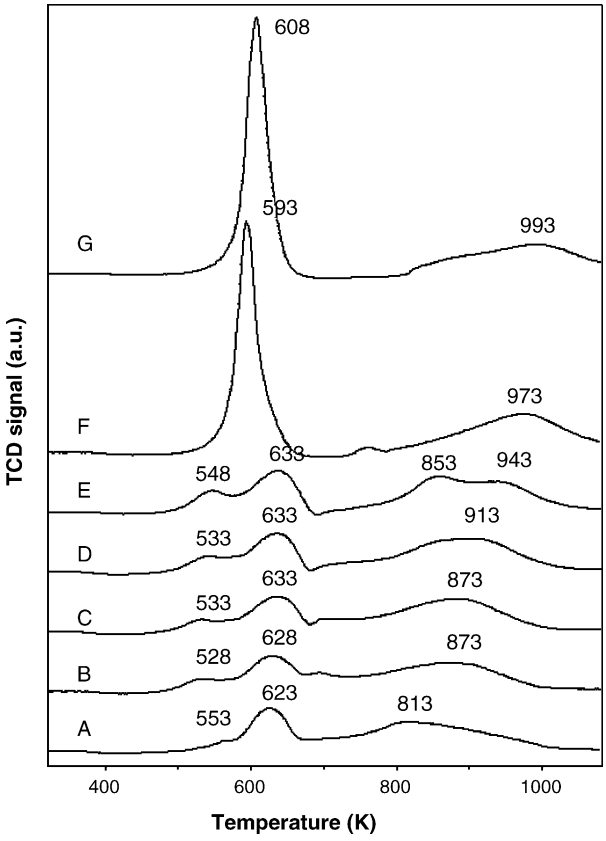

Fig. 5. TPR profiles of the prepared catalysts: (A) 15CoA; (B) 15Co03MA; (C) 15Co08MA; (D) 15Co2MA; (E) 15Co5MA; (F) 15Co9MA; (G) 15Co12MA.

density of the support layers when Co^{2+} is replaced by divalent cations of smaller ionic radius, such as Mg^{2+} [23].

Additional TPR experiments were carried out for the 15Co5Mg and 15Co12Mg samples, which were recalcined at 673 K for 5 h, to illustrate the effect of magnesia on the thermal stability of NO_3^- in the magnesia-modified catalysts, and the results are shown in Fig. 6. One can see that the narrow and intense peak at 608 K is actually attributed to the reductive decomposition of cobalt nitrate, which can only be entirely decomposed at 673 K.

It can also be observed that the reduction peaks at high temperature for magnesia-modified catalysts shift gradually to a higher temperature with increasing magnesia content. It has been suggested that this is due to a decrease in the reducibility of catalysts with the formation of a non-stoichiometric spinel phase containing Mg [22] or a CoO–MgO solid solution [18,38].

In general, the interaction between a metal oxide and a support may be classified into three categories [16]: (1) very weak interaction in which the support acts only as a dispersing agent, such as SiO_2-supported cobalt; (2) solid solution formation, such as CoO–MgO–Al_2O_3 system; (3) strong interaction or surface compound formation, such as TiO_2- or Al_2O_3-supported cobalt. In supported catalysts, the reducibility of the cobalt species often depends on the extent

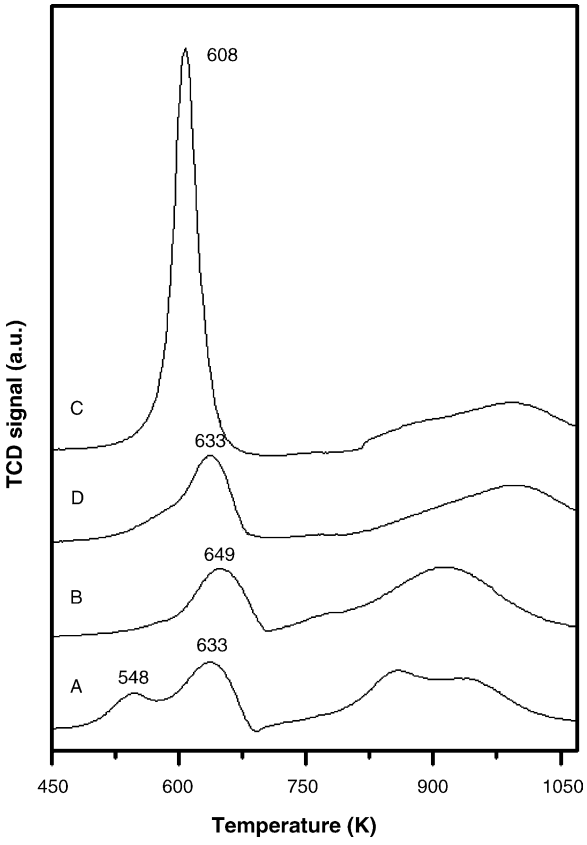

Fig. 6. TPR profiles of: (A) 15Co5MA; (B) 15Co5MA recalcined at 673 K for 5 h; (C) 15Co12MA; (D) 15Co12MA recalcined at 673 K for 5h.

of the metal–support interaction. The reduction temperature of the cobalt species depend on the nature and the amount of other cations in the catalyst due to the great ability of Co to be combined in spinel-like phases, and this is particularly true when the neighboring cations are Al and Mg [23].

LRS results indicated that CoO–MgO solid solution was formed in the prepared catalysts, it is believed that the formation of CoO–MgO solid solution affects the reduction of catalysts. In the TPR study, some CoO still exists in the catalyst above 623 K. The surface Mg/Al molar ratio of magnesia-modified catalysts obtained by XPS is much higher than its bulk ratio (see Table 1), indicating an enrichment of surface Mg in these catalysts. XPS study has shown that the addition of magnesia inhibited the major interaction between alumina and cobalt. However, magnesia may interact with cobalt to some extent in the TPR process. With increasing magnesia content, the surface Mg is more enriched than the bulk, and the interaction between MgO and CoO is enhanced with the formation of CoO–MgO solid solution above 623 K. This kind of cobalt species can only be reduced at an elevated temperature.

3.6. H_2 chemisorption and O_2 titration

The results of H_2 chemisorption (H_2-TPD) and O_2 titration are shown in Table 5. It is evident that H_2 chemisorption decreases significantly with increasing magnesia content. This indicates that the cobalt active sites decreased when large amounts of magnesia were added to the catalysts. Simultaneously, the percentage reduction of the catalyst increases slightly for low-magnesia content catalysts and decreases significantly for high-magnesia content catalysts. It is suggested that small amounts of magnesia could suppress the interaction between the cobalt and the support, and the reducibility of the catalysts was improved. At higher magnesia content catalysts, the reducibility of the catalysts decreased due to the interaction between magnesia and cobalt oxide with formation of CoO–MgO solid solution. This result has also been revealed by our LRS, XPS and TPR experiments.

It can also be seen that the corrected cobalt dispersion of magnesia-modified catalysts is lower than that of the unmodified catalyst, but is independent of magnesia content. The XPS results also indicated that addition of magnesia inhibited the formation of cobalt surface phase, which is highly dispersed on the support. It is suggested that the decrease of highly dispersed species induced the decrease of cobalt dispersion.

Furthermore, the cobalt cluster size increases with addition of magnesia and is independent of the amount of magnesia. This is consistent with the XRD results (see Table 5).

Table 5
H_2 chemisorption (H_2-TPD) and O_2 titration results

Samples name	H_2 desorbed (μmol g^{-1})	Uncorrected D%[d]	Uncorrected diameter[a,d] (nm)	Red.%[c]	Corrected D%[e]	Corrected diameter[a,e] (nm)	Co_3O_4 diameter[b] (nm)
15CoA	93.6	7.36	14.0	51.43	14.31	7.2	18.3
15Co03MA	55.1	4.33	23.8	54.12	8.00	12.88	18.1
15Co08MA	56.6	4.44	23.2	56.16	7.90	13.03	18.7
15Co2MA	49.8	3.91	26.4	45.58	8.58	12.03	22.5
15Co5MA	44.8	3.52	29.3	41.31	8.52	12.10	20.2
15Co9MA	15.6	1.22	84.5	16.7	7.29	14.10	21.0
15Co12MA	14.5	1.14	90.4	13.6	8.39	12.30	21.8

[a] The cobalt cluster diameter.
[b] Average diameter of Co_3O_4 crystallite obtained by XRD measurement.
[c] Percentage reduction of catalysts.
[d] The data were uncorrected by percentage reduction.
[e] The data were corrected by percentage reduction.

Table 6
Catalytic performance data of the magnesia-modified Co/Al_2O_3 catalysts for FTS

Samples name	CO conversion (%)	CO_2 selectivity (%)	Hydrocarbon selectivity (%)				
			CH_4	C_2	C_3	C_4	C_5^+
15CoA	32.06	1.09	16.23	1.52	2.04	1.39	77.73
15Co03MA	32.07	1.53	18.54	1.12	1.81	1.34	75.67
15Co08MA	35.56	1.70	19.16	0.96	1.78	1.31	75.16
15Co2MA	24.67	1.76	20.56	1.34	1.89	1.44	73.20
15Co5MA	15.78	1.20	21.47	1.25	1.73	1.99	72.35
15Co9MA	7.15	1.37	19.94	1.32	1.75	1.81	73.82
15Co12MA	6.25	1.47	20.76	1.61	1.45	1.60	73.05

The catalysts were reduced in a flow of H_2 at 723 K for 16 h before FTS.
Reaction conditions: $H_2/CO = 2$; space velocity of syngas was 2 S L g^{-1} h^{-1} (273 K, 0.1 Mpa); temperature was 503 K; pressure was 10 bar.

3.7. Fischer–Tropsch synthesis (FTS)

The results of catalytic performances for FTS are listed in Table 6. Three trends are apparent from Table 6: (1) with increasing magnesia content, the CO conversion first increases slightly and then decreases; (2) the CO_2 and methane selectivities of magnesia-modified catalysts are higher than that of unmodified cobalt catalyst; (3) the C_5^+ hydrocarbon selectivity of the magnesia-modified catalysts is slightly lower than that of unmodified cobalt catalyst and mild decreases with increasing magnesia content.

It has been suggested that the activity of cobalt catalyst was directly dependent on the catalyst reducibility for FTS [39]. Thus, the trend in variation of CO conversion with magnesia content is similar to that of percentage reduction of the catalysts, and the higher CO_2 selectivity may also originate from the presence of more unreduced cobalt species, which are active for the water–gas shift [40].

The appropriate interaction between cobalt and alumina support can keep the stabilization of cobalt active sites during the FTS. However, a certain extent of cobalt surface reconstruction during the early initial reaction time by CO (in the presence of H_2) occurs. The self-organization procedure (reconstruction) of the cobalt surface, via segregation of the catalyst surface planes, plays a dominant role to increase activity and to change/improve selectivity, this should be regarded as an essential feature of FTS with cobalt [41,42]. By this process, the number of sites increases largely and the sites disproportionate into sites of lower and higher coordination on the expense of plane sites (on-top sites, in-hole sites and on-plane sites, respectively). These different sites would exhibit different catalytic properties in the FTS regime [41].

During the steady state of FTS, most of major reactions (chain growth, CO dissociation) are related to on-top sites and in-hole sites, whereas on-plane sites are widely poisoned through CO chemisorption. However, some extent minor reactions (olefin isomerization, olefin hydrogenation and methane formation) are related to these remaining plane sites, Moreover, olefin readsorption, which generally leads to modification of product distribution, is an important olefin secondary reaction on growth sites (on-top sites) [43].

From discussion above, the interaction between MgO and CoO is enhanced with the formation of CoO–MgO solid solution during reduction of catalyst; thereby, it is understood that MgO could suppress the process of reconstruction of the cobalt surface under FTS conditions, this conduces sites to remain on the plane sites or sites of higher coordination. Thus, the remaining plane sites to growth sites ratio increases with magnesia content increasing. Anyway, the loss of activity, lower C_5^+ hydrocarbon selectivity and excessive methane formation on higher magnesia-modified cobalt catalysts might be deduced from that MgO hinders the process of catalyst reassembling under FTS conditions.

Zhang et al. [44] have suggested that supports with lower acidity led to the higher activities, higher C_5^+ hydrocarbon selectivity and lower methane selectivity. The number of acidic sites on the magnesia-modified Al_2O_3 was higher than that of Al_2O_3 and the addition of magnesia can decrease the strong acidic sites and increase the weak acidic sites [45,46]. Thus, the increase in acidic sites with increasing magnesia content may also induce the poor catalytic performance, but this need further experiment to testify.

Fig. 7 clarifies the effect of the magnesia content on the olefin to paraffin ratio. The ratio of olefin to paraffin decreases with increasing chain length for all catalysts, and a significant trend can be observed that the ratio of olefin to paraffin increases with increasing magnesia content.

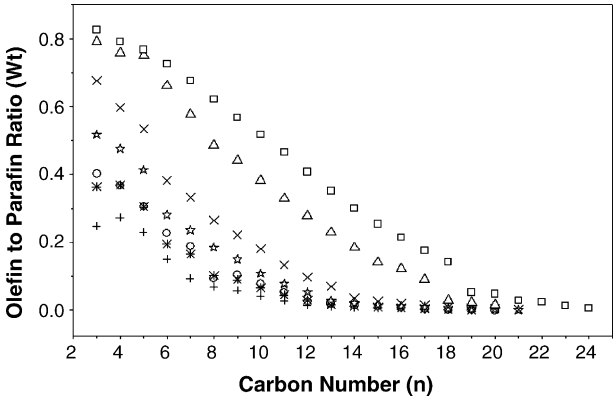

Fig. 7. Effect of the magnesia content on the olefin to paraffin ratio: (+) 15CoA; (◯) 15Co03MA; (✳) 15Co08MA; (☆) 15Co2MA; (×) 15Co5MA; (△) 15Co9MA; (□) 15Co12MA.

Schulz and Claeys [47] have suggested that the change of olefin selectivity (olefin to paraffin ratio) could be well described as an effect of the olefin readsorption on the on-top (growth) sites probability, which due to the different residence times of reaction products. It should further be noted that the chain length-dependent reaction products solubility, which increases with increasing carbon number, has the governing effect on chain length-dependent residence times of reaction products in the liquid-filled pores of the catalyst [48]. Iglesia and co-workers [49] advanced that the decrease in pore volume of catalyst can induce a decrease in pore residence time of reaction products, further causing a decrease in olefin readsorption. Thus, the olefin selectivity increases.

The total pore volume of catalysts decreases with increasing magnesia content at present study (see Table 2). However, the inhibition secondary olefin reactions (olefin readsorption), which deduces from a decrease in the on-top growth sites to remaining plane sites ratio via that MgO hinders the surface reconstruction of cobalt catalysts during initial reaction time, could has a major effect on the magnesia content-dependent olefin selectivity.

4. Conclusions

The effect of magnesia on Co/Al_2O_3 FTS catalysts has been investigated.

It was evident that the formation of a cobalt surface phase, which strongly interacts with the alumina support, can be effectively suppressed by modification of a small amount of magnesia. Large amounts of magnesia restrained the reduction of the catalysts due to the formation of MgO–CoO solid solution.

The activity of low magnesia-modified catalysts for FTS increased due to an increase in catalyst reducibility. However, lower activity, lower C_5^+ hydrocarbon selectivity, higher methane and CO_2 selectivities were obtained for higher magnesia content catalysts, these can be described as an effect of a decrease in catalyst reducibility and/or magnesia content-dependent catalyst surface reconstruction suppression, which also has a dominant effect on the magnesia content-dependent olefin selectivity. Moreover, a feasible explanation of the carbon number-dependent olefin to paraffin ratio might be chain length-dependent reaction products solubility

It is known that a possible deactivation route of cobalt-based catalysts is due to the presence of water vapor, which induced the compound formation between cobalt metal and the support under reaction conditions. Thus, further work is needed to determine the role of magnesia in the deactivation of cobalt base FTS catalysts.

Acknowledgements

This work was supported by the National Natural Science Foundation of China (20373090, 20473114, 20590360), Talented Young Scientist Foundation of Hubei (2003ABB013), Excellent Young Teachers Program of Ministry of Education of China, the State Ethnic Affairs Commission of China and Returnee Startup Scientific Research Foundation of Ministry of Education of China.

References

[1] H. Schulz, Appl. Catal. A 186 (1999) 3.
[2] R.B. Anderson, Fischer–Tropsch Synthesis, Academic Press, NY, 1984.
[3] M.E. Dry, Catal. Today 71 (2002) 227.
[4] J.L. Zhang, J.G. Chen, J. Ren, Y.H. Sun, Appl. Catal. A 243 (2003) 121.
[5] G. Jacobs, T.K. Das, Y.Q. Zhang, J.L. Li, G. Racoillet, B.H. Davis, Appl. Catal. A 233 (2002) 263.
[6] J.L. Li, G. Jacobs, T.K. Das, Y.Q. Zhang, B.H. Davis, Appl. Catal. A 236 (2002) 67.
[7] R.C. Reuel, C.H. Bartholomew, J. Catal. 85 (1984) 78.
[8] E. Iglesia, S.L. Soled, R.A. Fiato, G.H. Via, J. Catal. 143 (1993) 345.
[9] D. Schanke, S. Vada, E.A. Blekkan, A.M. Hilmen, A. Hoff, A. Holmen, J. Catal. 156 (1995) 85.
[10] A. Kogelbauer, J.G. Goodwin, R.J. Oukaci, J. Catal. 160 (1996) 125.
[11] P. Arnoldy, J.A. Moulijn, J. Catal. 93 (1985) 38.
[12] R.L. Chin, D.M. Hercules, J. Phys. Chem. 86 (1982) 360.
[13] J.L. Li, X.D. Zhan, Y.Q. Zhang, G. Jacobs, T. Das, B.H. Davis, Appl. Catal. A 228 (2002) 203.
[14] T.K. Das, G. Jacobs, P.M. Patterson, W.A. Conner, J.L. Li, B.H. Davis, Fuel 82 (2003) 805.
[15] G.R. Moradi, M.M. Basir, A. Taeb, A. Kiennemann, Catal. Commun. 4 (2003) 27.
[16] W.J. Wang, Y.W. Chen, Appl. Catal. 77 (1991) 223.
[17] P.A. Chernavskii, G.V. Pankina, V.V. Lunin, Catal. Lett. 66 (2000) 121.
[18] M.K. Niemelä, A.O.I. Krause, Catal. Lett. 34 (1995) 75.
[19] B.A. Sexton, A.E. Hughes, T.W. Turney, J. Catal. 97 (1986) 390.
[20] M.K. Niemelä, A.O.I. Krause, T. Vaara, J. Lahtinen, Top. Catal. 2 (1995) 45.
[21] A.L. Lapidus, I.A. Bruk, V.V. Mal'tsev, C.Y. Khoang, V.I. Yakerson, E.Z. Golosman, I.A. Mamaeva, Petrol. Chem. 21 (6) (1981) 863.
[22] H. Schulz, E. van Steen, M. Claeys, Stud. Surf. Sci. Catal. 81 (1994) 455.
[23] S. Ribet, D. Tichit, B. Coq, B. Ducourant, F. Morato, J. Solid State Chem. 142 (1999) 382.
[24] J. Lahtinen, G.A. Somorjai, J. Mol. Catal. A 130 (1998) 255.
[25] A.M. Hilmen, D. Schanke, K.F. Hanssen, A. Holmen, Appl. Catal. A 186 (1999) 169.
[26] H.F. Xiong, Y.H. Zhang, K.Y. Liew, J.L. Lin, J. Mol. Catal. A 231 (2005) 145.
[27] B.D. Cullity, Elements of X-ray Diffraction, third ed., Addison-Wesley, Reading, MA, 1967.
[28] D. Schanke, S. Vada, E.A. Blekkan, A.M. Hilmen, J. Catal. 156 (1995) 85.
[29] R.C. Reuel, C.H. Bartholomew, J. Catal. 85 (1984) 63.
[30] D.E. Jiang, B.Y. Zhao, Y.C. Xie, G.C. Pan, G.P. Ran, E. Min, Appl. Catal. A 219 (2001) 69.
[31] B. Jongsomjit, J. Panpranot, J.G. Goodwin Jr., J. Catal. 204 (2001) 98.
[32] T.C. Xiao, S.F. Ji, H.T. Wang, K.S. Coleman, Malcolm L.H. Green, J. Mol. Catal. A 175 (2001) 111.
[33] M.A. Ulla, R. Spretz, E. Lombardo, W. Daniell, H. Knözinger, Appl. Catal. B 29 (2001) 217.
[34] M. Oku, K. Hirokawa, J. Electron. Spectrosc. 8 (1976) 475.

[35] L. Ji, J. Lin, H.C. Zeng, J. Phys. Chem. B 104 (2000) 1783.
[36] Z. Zsoldos, T. Hoffer, L. Guczi, J. Phys. Chem. 95 (1991) 798.
[37] Z. Zsoldos, L. Guczi, J. Phys. Chem. 96 (1992) 9393.
[38] R.B. Anderson, in: P.H. Emmett (Ed.), Catalysis, vol. IV, Reinhold, NY, 1956, p. 82 (Chapter 2).
[39] A.R. Belambe, R. Oukaci, J.G. Goodwin Jr., J. Catal. 166 (1997) 8.
[40] J.L. Li, N.J. Coville, Appl. Catal. A 181 (1999) 201.
[41] H. Schulz, Z. Nie, F. Qusmanov, Catal. Today 71 (2002) 351.
[42] J.J.C. Geerlings, J.H. Wilson, G.J. Kramer, H.P.C.E. Kuipers, A. Hoek, H.M. Huisman, Appl. Catal. A 186 (1999) 27.
[43] H. Schulz, Topics Catal. 26 (2003) 73.
[44] J.L. Zhang, J.G. Chen, J. Ren, Y.W. Li, Y.H. Sun, Fuel 82 (2003) 581.
[45] H. Tsuji, F. Yagi, H. Hattori, H. Kita, J. Catal. 148 (1994) 759.
[46] J.Y. Shen, R.D. Cortright, Y. Chen, J.A. Dumesic, J. Phys. Chem. 98 (1994) 8067.
[47] H. Schulz, M. Claeys, Appl. Catal. A 186 (1999) 91.
[48] H. Schulz, M. Claeys, Appl. Catal. A 186 (1999) 71.
[49] R.J. Madon, S.C. Reyes, E. Iglesia, J. Phys. Chem. 95 (1991) 7795.